# A Mixed Spectral-Domain Approach for Dispersion Analysis of Suspended Planar Transmission Lines with Pedestals

CHI HOU CHAN, MEMBER, IEEE, KWONG T. NG, MEMBER, IEEE, AND AMMAR B. KOUKI, STUDENT MEMBER, IEEE

*Abstract* — **A mixed spectral-domain analysis is used to derive dispersion characteristics of dominant modes in a class of planar transmission lines with a pedestal. Equivalent structures are constructed in which magnetic surface currents are identified as the unknowns at the aperture separating two different regions. Spectral dyadic Green's functions are derived for these structures using the spectral-domain immittance approach. The characteristic equations resulting from the application of the spectral Galerkin method involve mixing two different spectral domains, which exist on the two sides of the pedestal support. The present method allows one to retain the simplicity and numerical efficiency of the conventional spectral-domain immittance approach, which cannot be applied directly to the present structures. Numerical data are provided for the dispersion characteristics of dominant modes in a pedestal-supported stripline and finline.**

## I. INTRODUCTION

SUSPENDED striplines have been increasingly used as transmission structures in various millimeter-wave components [1]–[3]. The ease with which they can be fabricated and their planar configuration make them suitable for integrating into monolithic millimeter-wave integrated circuits. At the same time, compared with the conventional microstrip line, they offer lower propagation losses and wider strips (for a given impedance), which make them more tolerant to the manufacturing process. It was also believed that they are less dispersive. However, as pointed out in [4], the dispersion is not always negligible. Thus, a frequency-dependent solution is important for suspended striplines.

The substrate in a suspended stripline can be supported by either grooves or pedestals [5]. As pointed out in [3], with comparable dielectric and channel dimensions, the pedestal-supported suspended stripline exhibits a substantially higher moding frequency than the suspended stripline with a groove (even higher than the conventional microstrip), giving it a much wider usable frequency range. Also, the pedestal-supported suspended stripline has a larger impedance range for given strip widths than does the microstrip. Further, when compared with a groove-supported suspended stripline of similar dimensions, the structure with a pedestal gives an impedance which is less sensitive to dimensional tolerances, especially for wide strips [3]. These considerations are important for millimeter-wave component designs, e.g., filter designs [3].

The finline is another class of planar transmission line widely used in millimeter-wave components [6], [7]. They have several advantages: (1) low-loss propagation; (2) relatively wide single-mode bandwidth, as the finline somewhat resembles the ridged waveguide; (3) compatibility with beam-lead and chip devices, thus again offering the potential for integrating into monolithic millimeter-wave integrated circuits; and (4) longer guide wavelength when compared to a microstrip, thus giving larger dimensional tolerances. Again, the dielectric substrates in finlines have to be supported by grooves or pedestals as in suspended striplines.

The suspended stripline and finline, without any support structure, have been analyzed with different methods, including the spectral-domain approach [8], [9]. However, only quasi-static analyses for the pedestal-supported stripline are available [3], [5]. As for the finline, a frequency-dependent analysis incorporating the support structure has been performed with a hybrid-mode mode-matching technique in the spatial domain [10]. More recently, an asymmetrical finline has been analyzed with a spectral-domain technique [11]. In this paper, frequency-dependent analyses are presented for a class of suspended striplines and finlines with pedestals. A generalization of the spectral-domain immittance approach for conventional planar transmission lines [12] is used. The new approach takes into account the fact that the regions above and below the pedestal support have different sidewall separations; hence, it requires the mixing of two different spectral domains which exist on the two sides of the pedestal support. The major difference between the present method

Manuscript received November 28, 1988; revised June 26, 1989. This work was supported by a contract (F19628-88-K0019) from the Rome Air Development Center to K. T. Ng.

C. H. Chan was with the Electromagnetic Communication Laboratory, Department of Electrical and Computer Engineering, University of Illinois, Urbana, IL. He is now with the Department of Electrical Engineering, University of Washington, Seattle, WA 98195.

K. T. Ng is with the Applied Electromagnetics Laboratory, Department of Electrical Engineering, University of Virginia, Charlottesville, VA 22901.

A. B. Kouki is with the Electromagnetic Communication Laboratory, Department of Electrical and Computer Engineering, University of Illinois, Urbana, IL 61801.

IEEE Log Number 8930657.

0018-9480/89/1100-1716$01.00 ©1989 IEEE

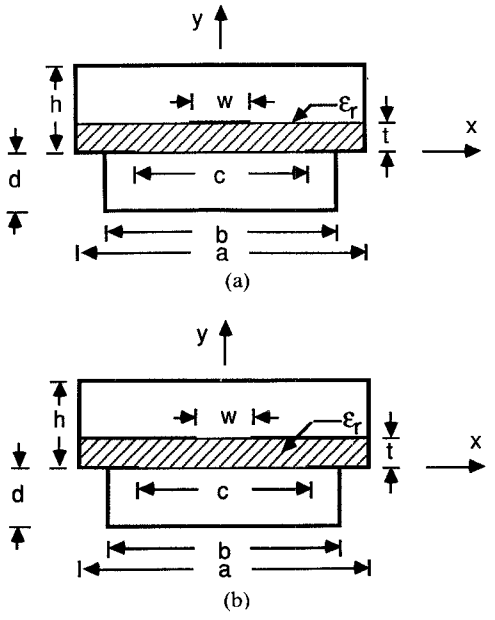


Fig. 1. Pedestal-supported transmission lines. (a) Stripline. (b) Finline.

and the one described in [11] is that the attractive essential features of the spectral-domain immittance approach are retained in formulating the characteristic equations for the dispersion analysis of quasi-planar transmission lines. As pointed out later, the method itself is quite general; hence, it is applicable to other structures, e.g., transmission lines with finite metallization thickness and substrate holding grooves.

## II. Formulation

Fig. 1(a) and (b) depicts the pedestal-supported stripline and finline. The major difference between the present structures and those discussed in [12] and [13] is that the sidewalls in this case have different separations for $y$ greater than and less than zero. As a result, the spectral-domain immittance approach described in [12] and [13] cannot be applied directly to the present problems, as the Fourier transform variable $\alpha$ in $x$ has different values for $y$ greater than and less than zero, in order to satisfy the boundary conditions on the electric walls. The spectral-domain immittance approach, however, can be applied to the auxiliary problems shown in Figs. 2 and 3.

For the pedestal-supported stripline, as shown in Fig. 2(a), the aperture at the $y=0$ plane is replaced by a perfectly conducting plane (shorted aperture), with the original tangential electric field at the aperture restored at $y=0^+$ and $y=0^-$ by appropriate magnetic surface currents $\boldsymbol{M}$ and $-\boldsymbol{M}$, respectively. The metallic strip, on the other hand, is replaced by an electric surface current $\boldsymbol{J}$. One can write expressions for the magnetic field above and below the $y=0$ plane. Following the procedure in [14], the total transverse magnetic field at the $y=0^+$ plane is the sum of the field radiated by $\boldsymbol{M}$ in the presence of the shorted aperture and the short-circuited field due to $\boldsymbol{J}$ (see Fig. 2(b)). On the other hand, the field at $y=0^-$ is radiated by $-\boldsymbol{M}$ in the presence of the conducting plane

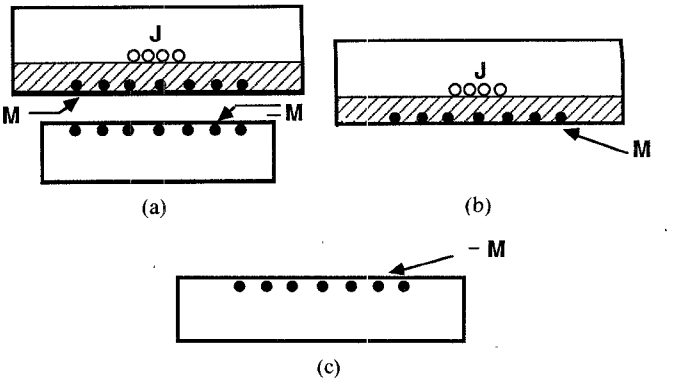


Fig. 2. Equivalent structures for obtaining fields for a pedestal-supported stripline. (a) Equivalent magnetic current with a shorted aperture. (b) Equivalent structure valid for the field above the $y=0$ plane. (c) Equivalent structure valid for the field below the $y=0$ plane.

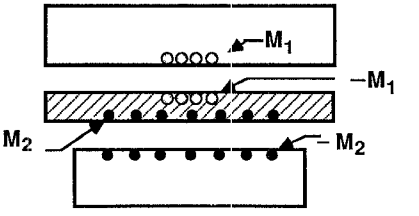


Fig. 3. Equivalent structure for obtaining fields for pedestal-supported finline.

and the environment for the region $y<0$ (see Fig. 2(c)). The electric field at the $y=t$ plane can also be found for the equivalent structure shown in Fig. 2(b). One can use the conventional spectral-domain immittance approach to derive the appropriate spectral Green's functions for these equivalent structures. The enforcement of continuity of the transverse magnetic field across the aperture relates the unknown magnetic surface current $\boldsymbol{M}$ and the electric surface current $\boldsymbol{J}$. For the pedestal-supported finline, one can again replace the apertures at $y=0$ and $t$ with conducting planes and magnetic surface currents as shown in Fig. 3. The continuity of the transverse magnetic field across the apertures is again enforced. Each of the field quantities in the equivalent structures can be derived using the conventional spectral-domain immittance approach.

The spectral-domain immittance approach is well documented in the literature [12], [13]; hence, only the final expressions for the fields are given here. However, we wish to mention an important point in adapting the approach to magnetic surface currents. With the coordinates $u$ and $v$ defined as in [12], then, in the case of electric surface current, the $\tilde{J}_u$ current ($u$ component in the transform domain) creates only TE-to-$y$ fields and the $\tilde{J}_v$ current ($v$ component in the transform domain) creates only TM-to-$y$ fields [12]. With magnetic surface current, on the other hand, the $\tilde{M}_u$ current creates only the TM fields while the $\tilde{M}_v$ current creates only the TE fields.

With all the appropriate variables defined in the Appendix, fields at $y=0$ and $t$ in the transform domain and boundary conditions applied in the spectral Galerkin method are given as follows. Quantities with a tilde ( ~ )

are Fourier transforms of corresponding quantities without a tilde. The Fourier transform is defined as in [12] and [13]. The discrete transform variable is $p\pi/a$ and $q\pi/b$ for $y > 0$ and $y < 0$, respectively.

### A. Stripline

At $y = 0^+$, the transverse magnetic field due to the magnetic current $\boldsymbol{M}$ at $y = 0^+$ in the presence of the shorted aperture is

$$\begin{bmatrix} \tilde{H}_x \\ \tilde{H}_z \end{bmatrix}_{0^+} = \begin{bmatrix} \tilde{G}^1_{xx} & \tilde{G}^1_{xz} \\ \tilde{G}^1_{zx} & \tilde{G}^1_{zz} \end{bmatrix} \begin{bmatrix} \tilde{M}_x \\ \tilde{M}_z \end{bmatrix} = \begin{bmatrix} -Y^{1h}N_x^2 - Y^{1e}N_z^2 & (Y^{1e} - Y^{1h})N_xN_z \\ (Y^{1e} - Y^{1h})N_xN_z & -Y^{1e}N_x^2 - Y^{1h}N_z^2 \end{bmatrix} \begin{bmatrix} \tilde{M}_x \\ \tilde{M}_z \end{bmatrix} \tag{1}$$

and the short-circuited field due to the electric current $\boldsymbol{J}$ at $y = t$ is

$$\begin{bmatrix} \tilde{H}_x^{sc} \\ \tilde{H}_z^{sc} \end{bmatrix}_{0^+} = \begin{bmatrix} \tilde{G}^2_{xx} & \tilde{G}^2_{xz} \\ \tilde{G}^2_{zx} & \tilde{G}^2_{zz} \end{bmatrix} \begin{bmatrix} \tilde{J}_x \\ \tilde{J}_z \end{bmatrix} = \begin{bmatrix} (-Y^{2e} + Y^{2h})N_xN_z & -Y^{2e}N_z^2 - Y^{2h}N_x^2 \\ Y^{2h}N_z^2 + Y^{2e}N_x^2 & (-Y^{2h} + Y^{2e})N_xN_z \end{bmatrix} \begin{bmatrix} \tilde{J}_x \\ \tilde{J}_z \end{bmatrix}. \tag{2}$$

On the other hand, the magnetic current $-\boldsymbol{M}$ at $y = 0^-$ yields

$$\begin{bmatrix} \tilde{H}_x \\ \tilde{H}_z \end{bmatrix}_{0^-} = \begin{bmatrix} \tilde{G}^3_{xx} & \tilde{G}^3_{xz} \\ \tilde{G}^3_{zx} & \tilde{G}^3_{zz} \end{bmatrix} \begin{bmatrix} \tilde{M}_x \\ \tilde{M}_z \end{bmatrix} = -\begin{bmatrix} -Y^{3h}N_x^2 - Y^{3e}N_z^2 & (Y^{3e} - Y^{3h})N_xN_z \\ (Y^{3e} - Y^{3h})N_xN_z & -Y^{3h}N_z^2 - Y^{3e}N_x^2 \end{bmatrix} \begin{bmatrix} \tilde{M}_x \\ \tilde{M}_z \end{bmatrix}. \tag{3}$$

Enforcing the continuity of the transverse magnetic field across the aperture at $y = 0$ in the spatial domain, we have

$$\begin{bmatrix} H_x \\ H_z \end{bmatrix}_{0^+} + \begin{bmatrix} H_x^{sc} \\ H_z^{sc} \end{bmatrix}_{0^+} = \begin{bmatrix} H_x \\ H_z \end{bmatrix}_{0^-}. \tag{4}$$

Note that (4) is not valid in the transform domain when the different quantities are replaced by their Fourier transforms. This is due to the different spectral domains (different discrete transform variables) existing for $y = 0^+$ and $y = 0^-$, which are associated with different sidewall separations.

At $y = t$, the transverse electric field due to the electric and magnetic currents is

$$\begin{bmatrix} \tilde{E}_x \\ \tilde{E}_z \end{bmatrix}_t = \begin{bmatrix} \tilde{G}^4_{xx} & \tilde{G}^4_{xz} \\ \tilde{G}^4_{zx} & \tilde{G}^4_{zz} \end{bmatrix} \begin{bmatrix} \tilde{J}_x \\ \tilde{J}_z \end{bmatrix} + \begin{bmatrix} \tilde{G}^5_{xx} & \tilde{G}^5_{xz} \\ \tilde{G}^5_{zx} & \tilde{G}^5_{zz} \end{bmatrix} \begin{bmatrix} \tilde{M}_x \\ \tilde{M}_z \end{bmatrix} = \begin{bmatrix} Z^{4e}N_x^2 + Z^{4h}N_z^2 & (Z^{4e} - Z^{4h})N_xN_z \\ (Z^{4e} - Z^{4h})N_xH_z & Z^{4e}N_z^2 + Z^{4h}N_x^2 \end{bmatrix} \begin{bmatrix} \tilde{J}_x \\ \tilde{J}_z \end{bmatrix} + \begin{bmatrix} (P^{5h} - P^{5e})N_xN_z & P^{5e}N_x^2 + P^{5h}N_z^2 \\ -P^{5e}N_z^2 - P^{5h}N_x^2 & (P^{5e} - P^{5h})N_xN_z \end{bmatrix} \begin{bmatrix} \tilde{M}_x \\ \tilde{M}_z \end{bmatrix}. \tag{5}$$

### B. Finline

The transverse magnetic fields at the planes $y = t$ and 0, approaching from either side of each plane, take the following forms:

$$\begin{bmatrix} \tilde{H}_x \\ \tilde{H}_z \end{bmatrix}_{t^+} = \begin{bmatrix} \tilde{G}^6_{xx} & \tilde{G}^6_{xz} \\ \tilde{G}^6_{zx} & \tilde{G}^6_{zz} \end{bmatrix} \begin{bmatrix} \tilde{M}_{1x} \\ \tilde{M}_{1z} \end{bmatrix} = \begin{bmatrix} -Y^{6h}N_x^2 - Y^{6e}N_z^2 & (Y^{6e} - Y^{6h})N_xN_z \\ (Y^{6e} - Y^{6h})N_xH_z & -Y^{6h}N_z^2 - Y^{6e}N_x^2 \end{bmatrix} \begin{bmatrix} \tilde{M}_{1x} \\ \tilde{M}_{1z} \end{bmatrix} \tag{6}$$

$$\begin{bmatrix} \tilde{H}_x \\ \tilde{H}_z \end{bmatrix}_{t^-} = \begin{bmatrix} \tilde{G}^7_{xx} & \tilde{G}^7_{xz} \\ \tilde{G}^7_{zx} & \tilde{G}^7_{zz} \end{bmatrix} \begin{bmatrix} \tilde{M}_{1x} \\ \tilde{M}_{1z} \end{bmatrix} = -\begin{bmatrix} -Y^{7h}N_x^2 - Y^{7e}N_z^2 & (Y^{7e} - Y^{7h})N_xN_z \\ (Y^{7e} - Y^{7h})N_xN_z & -Y^{7h}N_z^2 - Y^{7e}N_x^2 \end{bmatrix} \begin{bmatrix} \tilde{M}_{1x} \\ \tilde{M}_{1z} \end{bmatrix} \tag{7}$$

$$\begin{bmatrix} \tilde{H}_x^{sc} \\ \tilde{H}_z^{sc} \end{bmatrix}_{t^-} = \begin{bmatrix} \tilde{G}^8_{xx} & \tilde{G}^8_{xz} \\ \tilde{G}^8_{zx} & \tilde{G}^8_{zz} \end{bmatrix} \begin{bmatrix} \tilde{M}_{2x} \\ \tilde{M}_{2z} \end{bmatrix} = -\begin{bmatrix} Y^{8h}N_x^2 + Y^{8e}N_z^2 & (Y^{8h} - Y^{8e})N_xN_z \\ (Y^{8h} - Y^{8e})N_xN_z & Y^{8h}N_z^2 + Y^{8e}N_x^2 \end{bmatrix} \begin{bmatrix} \tilde{M}_{2x} \\ \tilde{M}_{2z} \end{bmatrix} \tag{8}$$

$$\begin{bmatrix} \tilde{H}_x \\ \tilde{H}_z \end{bmatrix}_{0^+} = \begin{bmatrix} \tilde{G}^9_{xx} & \tilde{G}^9_{xz} \\ \tilde{G}^9_{zx} & \tilde{G}^9_{zz} \end{bmatrix} \begin{bmatrix} \tilde{M}_{2x} \\ \tilde{M}_{2z} \end{bmatrix} = -\begin{bmatrix} Y^{7h}N_x^2 + Y^{7e}N_z^2 & (Y^{7h} - Y^{7e})N_xN_z \\ (Y^{7h} - Y^{7e})N_xN_z & Y^{7h}N_z^2 + Y^{7e}N_x^2 \end{bmatrix} \begin{bmatrix} \tilde{M}_{2x} \\ \tilde{M}_{2z} \end{bmatrix} \tag{9}$$

$$\begin{bmatrix} \tilde{H}_x^{sc} \\ \tilde{H}_z^{sc} \end{bmatrix}_{0^+} = \begin{bmatrix} \tilde{G}^{10}_{xx} & \tilde{G}^{10}_{xz} \\ \tilde{G}^{10}_{zx} & \tilde{G}^{10}_{zz} \end{bmatrix} \begin{bmatrix} \tilde{M}_{1x} \\ \tilde{M}_{1z} \end{bmatrix} = -\begin{bmatrix} -Y^{10h}N_x^2 - Y^{10e}N_z^2 & (Y^{10e} - Y^{10h})N_xN_z \\ (Y^{10e} - Y^{10h})N_xN_z & -Y^{10h}N_z^2 - Y^{10e}N_x^2 \end{bmatrix} \begin{bmatrix} \tilde{M}_{1x} \\ \tilde{M}_{1z} \end{bmatrix} \tag{10}$$

$$\begin{bmatrix} \tilde{H}_x \\ \tilde{H}_z \end{bmatrix}_{0^-} = \begin{bmatrix} \tilde{G}^3_{xx} & \tilde{G}^3_{xz} \\ \tilde{G}^3_{zx} & \tilde{G}^3_{zz} \end{bmatrix} \begin{bmatrix} \tilde{M}_{2x} \\ \tilde{M}_{2z} \end{bmatrix}. \tag{11}$$

Again, after enforcing the continuity of the transverse magnetic field across the apertures at $y = t$ and 0 in the spatial domain, we obtain

$$\begin{bmatrix} H_x \\ H_z \end{bmatrix}_{t^+} = \begin{bmatrix} H_x \\ H_z \end{bmatrix}_{t^-} + \begin{bmatrix} H_x^{sc} \\ H_z^{sc} \end{bmatrix}_{t^-} \tag{12}$$

$$\begin{bmatrix} H_x \\ H_z \end{bmatrix}_{0^+} + \begin{bmatrix} H_x^{sc} \\ H_z^{sc} \end{bmatrix}_{0^+} = \begin{bmatrix} H_x \\ H_z \end{bmatrix}_{0^-}. \tag{13}$$

To apply the spectral Galerkin method [15], we expand the unknown magnetic and electric surface currents with sets of known basis functions weighted with unknown coefficients. These basis functions are analytically Fourier transformable, and should contain the edge conditions that $J_z$ and $M_z$ are singular and $J_x$ and $M_x$ are zero at the edges of the strip or apertures. In this paper, we use the

basis functions provided in [16] and [17]. More comments on the choice of basis functions will follow shortly. To determine the unknown weighting coefficients, we complete the Galerkin's method by carrying out the testing procedures.

For the stripline, we can test the transverse magnetic field at the $y = 0$ plane (eq. (4)) and the electric field at the $y = t$ plane (eq. (5)) with the basis functions for the magnetic surface current $\boldsymbol{M}$ and electric surface current $\boldsymbol{J}$, respectively. Testing in the spatial domain is given by the integral $\int_{-L/2}^{L/2} f(x)g(x)\,dx$, where $f(x)$ is a basis function, $g(x)$ is a field quantity, $L = a$ for $y = t$ and $0^+$, and $L = b$ for $y = 0^-$. Note that the integration limits are different for the left-hand side and right-hand side of (4), which is possible because the basis functions for $\boldsymbol{M}$ are zero for $b/2 < |L| < a/2$, i.e., outside the aperture. Applying the Parseval theorem then allows us to replace each integral by an inner product defined in the transform domain as the summation of $\tilde{f}(\alpha)\tilde{g}(\alpha)/L$ over a discrete transform variable. (Thus, the inner product of the electric field and an electric current basis function at $y = t$ is zero as these two quantities are nonzero in complementary regions.) Similarly, for the finline, (12) and (13) are tested with the basis functions for the magnetic surface currents, $\boldsymbol{M}_1$ and $\boldsymbol{M}_2$, respectively. Then expressing the fields in terms of their spectral Green's functions, we obtain the following.

For stripline,

$$\frac{1}{a}\begin{bmatrix} \tilde{M}_x\tilde{G}^1_{xx}\tilde{M}_x & \tilde{M}_x\tilde{G}^1_{xz}\tilde{M}_z \\ \tilde{M}_z\tilde{G}^1_{zx}\tilde{M}_x & \tilde{M}_z\tilde{G}^1_{zz}\tilde{M}_z \end{bmatrix}_{\alpha_a}\begin{bmatrix} C_{Mx} \\ C_{Mz} \end{bmatrix} + \frac{1}{a}\begin{bmatrix} \tilde{M}_x\tilde{G}^2_{xx}\tilde{J}_x & \tilde{M}_x\tilde{G}^2_{xz}\tilde{J}_z \\ \tilde{M}_z\tilde{G}^2_{zx}\tilde{J}_x & \tilde{M}_z\tilde{G}^2_{zz}\tilde{J}_z \end{bmatrix}_{\alpha_a}\begin{bmatrix} C_{Jx} \\ C_{Jz} \end{bmatrix} = \frac{1}{b}\begin{bmatrix} \tilde{M}_x\tilde{G}^3_{xx}\tilde{M}_x & \tilde{M}_x\tilde{G}^3_{xz}\tilde{M}_z \\ \tilde{M}_z\tilde{G}^3_{zx}\tilde{M}_x & \tilde{M}_z\tilde{G}^3_{zz}M_z \end{bmatrix}_{\alpha_b}\begin{bmatrix} C_{Mx} \\ C_{Mz} \end{bmatrix} \quad (14)$$

$$\frac{1}{a}\begin{bmatrix} \tilde{J}_x\tilde{G}^4_{xx}\tilde{J}_x & \tilde{J}_x\tilde{G}^4_{xz}\tilde{J}_z \\ \tilde{J}_z\tilde{G}^4_{zx}\tilde{J}_x & \tilde{J}_z\tilde{G}^4_{zz}\tilde{J}_z \end{bmatrix}_{\alpha_a}\begin{bmatrix} C_{Jx} \\ C_{Jz} \end{bmatrix} + \frac{1}{a}\begin{bmatrix} \tilde{J}_x\tilde{G}^5_{xx}\tilde{M}_x & \tilde{J}_x\tilde{G}^5_{xz}\tilde{M}_z \\ \tilde{J}_z\tilde{G}^5_{zx}\tilde{M}_x & \tilde{J}_z\tilde{G}^5_{zz}\tilde{M}_z \end{bmatrix}_{\alpha_a}\begin{bmatrix} C_{Mx} \\ C_{Mz} \end{bmatrix} = 0. \quad (15)$$

For finline,

$$\frac{1}{a}\begin{bmatrix} \tilde{M}_{1x}\tilde{G}^6_{xx}\tilde{M}_{1x} & \tilde{M}_{1x}\tilde{G}^6_{xz}\tilde{M}_{1z} \\ \tilde{M}_{1z}\tilde{G}^6_{zx}\tilde{M}_{1x} & \tilde{M}_{1z}\tilde{G}^6_{zz}\tilde{M}_{1z} \end{bmatrix}_{\alpha_a}\begin{bmatrix} C_{M1x} \\ C_{M1z} \end{bmatrix} = \frac{1}{a}\begin{bmatrix} \tilde{M}_{1x}\tilde{G}^7_{xx}\tilde{M}_{1x} & \tilde{M}_{1x}\tilde{G}^7_{xz}\tilde{M}_{1z} \\ \tilde{M}_{1z}\tilde{G}^7_{zx}\tilde{M}_{1x} & \tilde{M}_{1z}\tilde{G}^7_{zz}\tilde{M}_{1z} \end{bmatrix}_{\alpha_a}\begin{bmatrix} C_{M1x} \\ C_{M1z} \end{bmatrix} + \frac{1}{a}\begin{bmatrix} \tilde{M}_{1x}\tilde{G}^8_{xx}\tilde{M}_{2x} & \tilde{M}_{1x}\tilde{G}^8_{xz}\tilde{M}_{2z} \\ \tilde{M}_{1z}\tilde{G}^8_{zx}\tilde{M}_{2x} & \tilde{M}_{1z}\tilde{G}^8_{zz}\tilde{M}_{2z} \end{bmatrix}_{\alpha_a}\begin{bmatrix} C_{M2x} \\ C_{M2z} \end{bmatrix} \quad (16)$$

$$\frac{1}{a}\begin{bmatrix} \tilde{M}_{2x}\tilde{G}^{10}_{xx}\tilde{M}_{1x} & \tilde{M}_{2x}\tilde{G}^{10}_{xz}\tilde{M}_{1z} \\ \tilde{M}_{2z}\tilde{G}^{10}_{zx}\tilde{M}_{1x} & \tilde{M}_{2z}\tilde{G}^{10}_{zz}\tilde{M}_{1z} \end{bmatrix}_{\alpha_a}\begin{bmatrix} C_{M1x} \\ C_{M1z} \end{bmatrix} + \frac{1}{a}\begin{bmatrix} \tilde{M}_{2x}\tilde{G}^9_{xx}\tilde{M}_{2x} & \tilde{M}_{2x}\tilde{G}^9_{xz}\tilde{M}_{2z} \\ \tilde{M}_{2z}\tilde{G}^9_{zx}\tilde{M}_{2x} & \tilde{M}_{2z}\tilde{G}^9_{zz}\tilde{M}_{2z} \end{bmatrix}_{\alpha_a}\begin{bmatrix} C_{M2x} \\ C_{M2z} \end{bmatrix} = \frac{1}{b}\begin{bmatrix} \tilde{M}_{2x}\tilde{G}^3_{xx}\tilde{M}_{2x} & \tilde{M}_{2x}\tilde{G}^3_{xz}\tilde{M}_{2z} \\ \tilde{M}_{2z}\tilde{G}^3_{zx}\tilde{M}_{2x} & \tilde{M}_{2z}\tilde{G}^3_{zz}\tilde{M}_{2z} \end{bmatrix}_{\alpha_b}\begin{bmatrix} C_{M2x} \\ C_{M2z} \end{bmatrix}. \quad (17)$$

Here $C_M$ and $C_J$ are the weighting coefficients of the basis functions for the magnetic and electric surface currents, respectively. It should be noted that the summations over all spectral terms as well as the basis functions are omitted in (14)–(17) for simplicity. For sidewall separations of $a$ and $b$, the discrete Fourier transform variables in $x$ are $\alpha_a$ and $\alpha_b$, respectively, and they will be defined later when numerical results are presented. The propagation constant $\beta$ dependence of (14)–(17) is inherent in the spectral Green's functions $G$'s. The dispersion characteristics of these pedestal-supported striplines and finlines are then given by the eigenvalues of the matrix equations formed by (14) to (17). The above formulation can readily be extended to include the effect of substrate holding grooves, which are realized by reducing the sidewall separation in the region $y > t$ in Fig. 1(a) and in (b) from $a$ to $b'$. For the finline with substrate holding grooves, the pertinent eigenvalue equations are still (16) and (17) with $\alpha_a$ on the left-hand side of (16) replaced by $\alpha_{b'}$. However, for the stripline with substrate holding grooves, it is more convenient to use equivalent magnetic currents at $y = t$ than the electric current that has been employed in this paper. The detailed procedures for analyzing the stripline and finline with finite metallization thickness and substrate holding grooves will be reported in [18]. As a final note in this section, we would like to point out that due to the different formulation scenarios, (16) and (17) are different from [11, eqs. (29) and (30)] for an asymmetrical finline.

## III. Results

The dispersion characteristics of the dominant modes for the suspended stripline and finline with pedestals have been computed using the mixed spectral-domain approach. The $E_z$ components of the dominant modes in the stripline and finline structures are even and odd, respectively. The basis functions we use in (14) to (17) are defined as follows.

For stripline,

$$J_x = \sum_{i=1}^{r} C_{Jxi}\eta_{oi}(x, w/2) \quad (18)$$

$$J_z = \sum_{i=1}^{r} C_{Jzi}\zeta_{ei}(x, w/2) \quad (19)$$

$$M_x = \sum_{i=1}^{s} C_{Mxi}\eta_{ei}(x, c/2) \quad (20)$$

$$M_z = \sum_{i=1}^{s} C_{Mzi}\zeta_{oi}(x, c/2). \quad (21)$$

For finline,

$$M_{x1} = \sum_{i=1}^{r} C_{Mx1i}\eta_{oi}(x, w/2) \tag{22}$$

$$M_{z1} = \sum_{i=1}^{r} C_{Mz1i}\zeta_{ei}(x, w/2) \tag{23}$$

$$M_{x2} = \sum_{i=1}^{s} C_{Mx2i}\eta_{oi}(x, c/2) \tag{24}$$

$$M_{z2} = \sum_{i=1}^{s} C_{Mz2i}\zeta_{ei}(x, c/2). \tag{25}$$

Here

$$\zeta_{ei}(x,\tau) = \cos[(i-1)\pi(x/\tau+1)]\Big/\sqrt{1-(x/\tau)^2} \tag{26}$$

$$\zeta_{oi}(x,\tau) = \cos[(i-0.5)\pi(x/\tau+1)]\Big/\sqrt{1-(x/\tau)^2} \tag{27}$$

$$\eta_{ei}(x,\tau) = \sin[(i-0.5)\pi(x/\tau+1)]\Big/\sqrt{1-(x/\tau)^2} \tag{28}$$

$$\eta_{oi}(x,\tau) = \sin[i\pi(x/\tau+1)]\Big/\sqrt{1-(x/\tau)^2} \tag{29}$$

where $\tau = w/2, c/2$. The Fourier transforms of these basis functions are functions of zero-order Bessel functions of the first kind, sampled at $\alpha_\sigma = 2(n-0.5)\pi/\sigma$ for the stripline and $\alpha_\sigma = 2n\pi/\sigma$ for the finline, where $\sigma = a$ or $b$. However, at the pedestal support $y = 0$, when the aperture width $c$ is equal to the wall separation $b$ of the pedestal, the singularity of the field no longer behaves as $(|x|-\tau)^{-1/2}$ but rather as $(|x|-\tau)^{-1+\lambda}$. The singular coefficient $\lambda$ can be determined from the formula provided in [19]. As a result, for those basis functions corresponding to the field at $y = 0$, the square root which appears in (26) and (27), should be replaced by a $(1-\lambda)$th root. The Fourier transforms of these new basis functions are in terms of Bessel functions of order $(1-\lambda)/2$ [17], which are more difficult to evaluate than the zero-order ones. Numerical experiments have shown that there is no significant difference in the calculated dispersion characteristics regardless of whether the square root or $(1-\lambda)$th root is used when $b = c$; hence, the square root is chosen for the basis functions. Finally, for all the numerical results presented in this section, the number of basis functions is set at $r = s = 3$ for each unknown component of the electric or magnetic current.

To demonstrate the versatility of the present approach, we calculate the normalized propagation constants for a variety of stripline and finline configurations. First we compute the dispersion characteristic of the perturbed microstrip quasi-TEM mode of a microstrip slot line. Fig. 4 shows the dispersion characteristics for different slot widths. The results show excellent agreement with those of Itoh [12]. If we reduce the sidewall separation for the region below the slot to the slot width, we obtain the pedestal-supported stripline structure proposed in [3].

Fig. 5 shows the variation of the normalized propagation constant with the strip width of a pedestal-supported stripline. At 1 GHz, the results compare very well with the

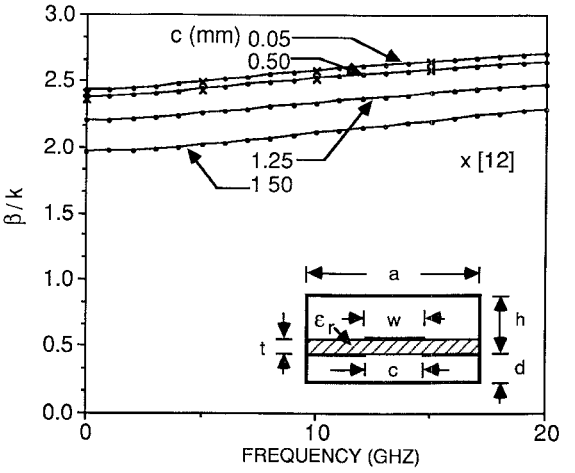


Fig. 4. Dispersion characteristics of microstrip slot lines; $a = 12.7$ mm, $d = 11.43$ mm, $t = 1.27$ mm, $h = 12.7$ mm, $w = 1.27$ mm, $\epsilon_r = 8.875$.

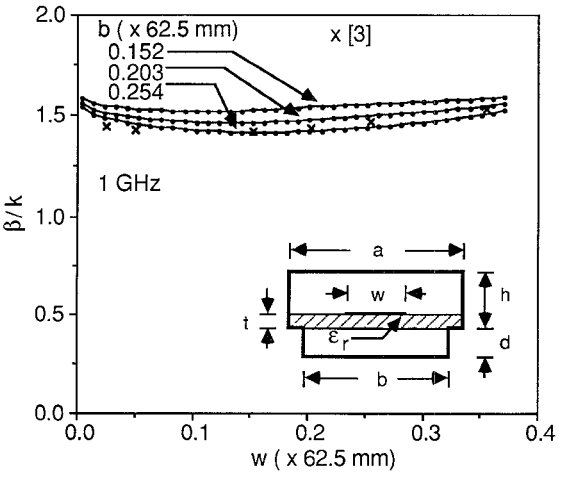


Fig. 5. Variation of the normalized propagation constant with the strip width of a pedestal-supported stripline; $a = 23.81$ mm, $d = 5.56$ mm, $t = 4.75$ mm, $h = 10.31$ mm, $\epsilon_r = 4.2$.

experimental values given in [3] for the slot width $b = 0.203 \times 62.5$ mm. Fig. 6 shows the dispersion characteristics of the pedestal-supported striplines with different slot widths. The results suggest that the quasi-static approximation employed in [3] may not be sufficient for higher frequencies. Fig. 7 shows more dispersion characteristics for the pedestal-supported striplines with alumina ($\epsilon_r = 8.8$) and GaAs ($\epsilon_r = 12.5$) substrates.

An asymmetrical finline with different sidewall separations on the two sides of the fin has been investigated recently in [11]. As illustrated in Fig. 8, this structure actually represents a special case of the pedestal-supported finline structure discussed in this paper. It should be noted that there are two apertures in the pedestal-supported finline and only one aperture in the asymmetrical finline. The frequency characteristic of the waveguide wavelength for the asymmetric finline shown in Fig. 8(a) has been computed in Table I. Excellent agreement (within 2 percent) with the experimental and theoretical results provided in [11] is obtained. Further, to demonstrate that the method is applicable to transmission lines with other sup-

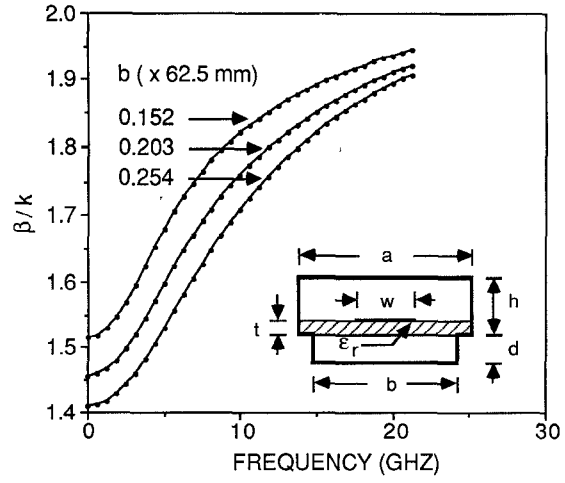


Fig. 6. Dispersion characteristics of a pedestal-supported stripline; $a = 23.81$ mm, $d = 5.56$ mm, $t = 4.75$ mm, $h = 10.31$ mm, $w = 9.5$ mm, $\epsilon_r = 4.2$.

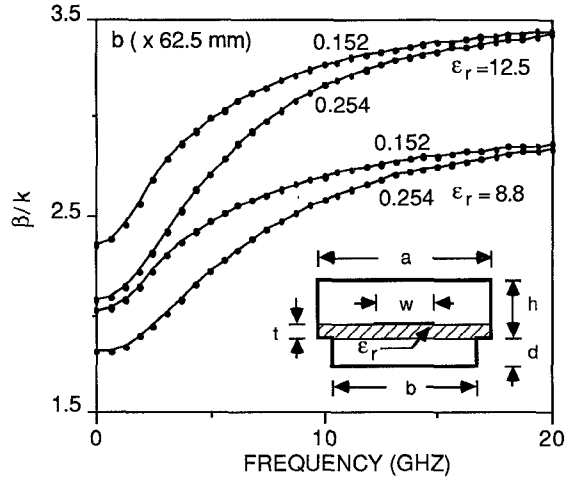


Fig. 7. Dispersion characteristics of a pedestal-supported stripline; $a = 23.81$ mm, $d = 5.56$ mm, $t = 4.75$ mm, $h = 10.31$ mm, $w = 9.5$ mm.

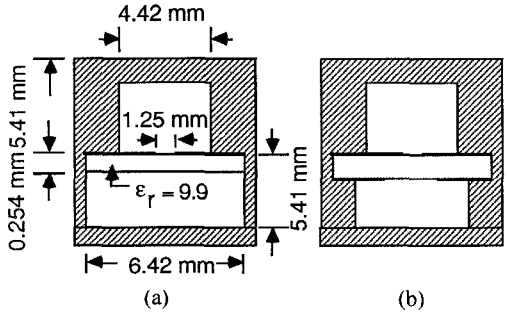


Fig. 8. Comparison between the asymmetrical finline and the pedestal-supported finline. (a) Asymmetrical finline studied in [11]. (b) Pedestal-supported finline.

port structures, the dispersion characteristics for a bilateral finline with a pedestal and a groove support are obtained as in Fig. 9. As one can see, the groove does not affect the dispersion characteristic of the finline, regardless of whether the separation is the same for the top and bottom sidewalls. Lastly, in Fig. 10, the dispersion characteristic of a pedestal-supported unilateral finline is compared with

TABLE I
THEORETICAL AND EXPERIMENTAL RESULTS FOR ASYMMETRICAL FINLINE

| Freq. (GHz) | $\lambda_g$ measured | $\lambda_g$ calculated | |
|---|---|---|---|
| | [11] | [11] | present method |
| 17.6 | 12.50 | 12.42 | 12.37 |
| 18.0 | 12.09 | 12.07 | 12.02 |
| 18.4 | 11.75 | 11.73 | 11.68 |
| 18.8 | 11.46 | 11 42 | 11.37 |
| 19.2 | 11.18 | 11.17 | 11.07 |
| 19.6 | 10.94 | 10 83 | 10.78 |
| 20.0 | 10.62 | 10.56 | 10.51 |

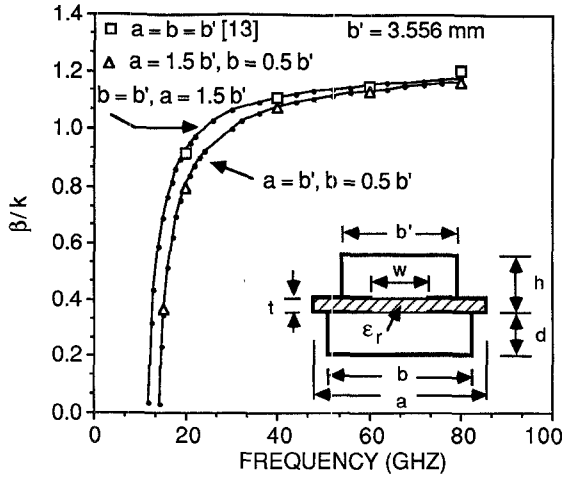


Fig. 9. Dispersion characteristics of bilateral finlines with different sidewall separations at different regions; $d = 3.4925$ mm, $t = 0.125$ mm, $h = 3.6185$ mm, $w = 0.5$ mm, $\epsilon_r = 3.75$.

the groove-supported unilateral finline. As the supporting region increases, the dispersion characteristics of the pedestal- and groove-supported unilateral finlines approach each other. Also shown in Fig. 10 are the dispersion characteristics of the groove-supported unilateral finlines with different slot widths. These results are within 2 percent of those given in [10] for a finline with a finite metallization thickness of 5 $\mu$m.

## IV. CONCLUSIONS

A mixed spectral-domain approach has been presented for the formulation of eigenvalue problems in the dispersion analysis of a suspended stripline and finline with pedestal support. The important feature of this approach is that we identify the magnetic surface currents as the unknowns at the aperture separating two different regions. This allows us to construct the eigenvalue solutions that require the mixing of two different spectral domains existing on opposite sides of the aperture at the pedestal support. Numerical results for different structures compare well with those obtained elsewhere with different methods. The present method is also applicable to the analysis of the stripline and finline with finite metallization thickness and substrate holding grooves, which will be reported in the near future.

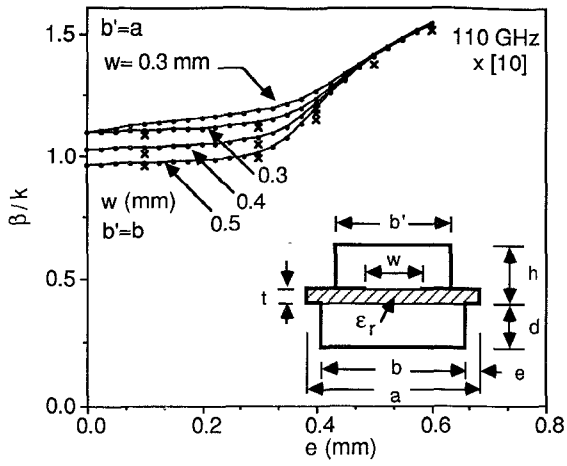


Fig. 10. Dispersion characteristics of pedestal-supported and groove-supported unilateral finlines; $b = 0.825$ mm, $d = 0.77$ mm, $t = 0.11$ mm, $h = 0.88$ mm, $\epsilon_r = 3.75$.

## Appendix

The variables that appear in the spectral dyadic Green's functions in (1) to (3) and (5) to (11) are given as

$$Y^{1e,h} = Y_2^{\mathrm{TM,TE}} \frac{Y_2^{\mathrm{TM,TE}} + Y_1^{e,h} \coth \gamma_2 t}{Y_1^{e,h} + Y_2^{\mathrm{TM,TE}} \coth \gamma_2 t} \tag{A1}$$

$$Y^{2e,h} = \frac{Y_2^{\mathrm{TM,TE}} / \sinh \gamma_2 t}{Y_1^{e,h} + Y_2^{\mathrm{TM,TE}} \coth \gamma_2 t} \tag{A2}$$

$$Y^{3e,h} = Y_3^{e,h} \tag{A3}$$

$$Z^{4e,h} = \frac{1}{Y_1^{e,h} + Y_2^{e,h}} \tag{A4}$$

$$P^{5e,h} = \frac{Y_2^{\mathrm{TM,TE}} / \sinh \gamma_2 t}{Y_1^{e,h} + Y_2^{\mathrm{TM,TE}} \coth \gamma_2 t} \tag{A5}$$

$$Y^{6e,h} = Y_1^{e,h} \tag{A6}$$

$$Y^{7e,h} = Y_2^{e,h} \tag{A7}$$

$$Y^{8e,h} = Y_2^{\mathrm{TM,TE}} / \sinh \gamma_2 t \tag{A8}$$

and

$$Y^{10e,h} = Y^{8e,h} \tag{A9}$$

where

$$Y_i^{\mathrm{TE}} = -\frac{\gamma_i}{j\omega\mu_0}, \qquad i = 1,2,3 \tag{A10}$$

$$Y_i^{\mathrm{TM}} = -\frac{j\omega\epsilon_0\epsilon_{ri}}{\gamma_i}, \qquad i = 1,2,3 \tag{A11}$$

$$\gamma_i = \left(\alpha^2 + \beta^2 - \epsilon_{ri} k_0\right)^{1/2}, \qquad i = 1,2,3 \tag{A12}$$

$$\epsilon_{r1} = \epsilon_{r3} = 1 \qquad \epsilon_{r2} = \epsilon_r \tag{A13}$$

$$Y_1^{e,h} = Y_1^{\mathrm{TM,TE}} \coth \gamma_1 (h - t) \tag{A14}$$

$$Y_2^{e,h} = Y_2^{\mathrm{TM,TE}} \coth \gamma_2 t \tag{A15}$$

$$Y_3^{e,h} = Y_3^{\mathrm{TM,TE}} \coth \gamma_3 d \tag{A16}$$

$$N_x = \frac{\alpha}{\sqrt{\alpha^2 + \beta^2}} \tag{A17}$$

and

$$N_z = \frac{\beta}{\sqrt{\alpha^2 + \beta^2}}. \tag{A18}$$

## Acknowledgment

Two of the authors, C. H. Chan and A. B. Kouki, gratefully acknowledge Prof. R. Mittra, Director of the Electromagnetic Communication Laboratory, University of Illinois, for his support and encouragement. Helpful discussion with R. E. Jorgenson is also appreciated. Further, K. T. Ng would like to acknowledge the Semiconductor Device Laboratory at the University of Virginia and the National Radio Astronomy Observatory, Charlottesville, VA, for their helpful discussions.

## References

[1] R. S. Tahim, G. M. Hayashibara, and K. Chang, "Design and performance of *W*-band broadband integrated circuit mixers," *IEEE Trans. Microwave Theory Tech.*, vol. MTT-31, pp. 277–283, Mar. 1983.

[2] S. K. Pan, M. J. Feldman, and A. R. Kerr, "Low-noise 115-GHz receiver using superconducting tunnel junctions," *Appl. Phys. Lett*, vol. 43, pp. 786–788, Oct. 1983.

[3] J. W. Archer, "An efficient 200–290-GHz frequency tripler incorporating a novel stripline structure," *IEEE Trans. Microwave Theory Tech.*, vol. MTT-32, pp. 416–420, Apr. 1984.

[4] R. S. Tomar and P. Bhartia, "Modeling the dispersion in a suspended microstripline," in *1987 IEEE MTT-S Int Microwave Symp. Dig.*, pp. 713–715.

[5] E. Yamashita, M. Nakajima, and K. Atsuki, "Analysis method for generalized suspended striplines," *IEEE Trans. Microwave Theory Tech.*, vol. MTT-34, pp. 1457–1463, Dec. 1986.

[6] R. N. Bates, S. J. Nightingale, and P. M. Ballard, "Millimeter-wave *E*-plane components and subsystems," *Radio Electron. Eng.*, vol. 52, pp. 506–512, Nov.–Dec. 1982.

[7] K. Solbach, "The status of printed mm-wave *E*-plane circuits," *IEEE Trans. Microwave Theory Tech.*, vol. MTT-31, pp. 107–121, Feb. 1983.

[8] T. Itoh, Ed., *Planar Transmission Line Structures* New York: IEEE Press, 1987.

[9] B. Bhat and S. K. Koul, *Analysis, Design and Applications of Fin Lines*. Norwood, MA: Artech House, 1987.

[10] R. Vahldieck, "Accurate hybrid-mode analysis of various finline configurations including multilayered dielectrics, finite metallization thickness, and substrate holding grooves," *IEEE Trans. Microwave Theory Tech.*, vol. MTT-32, pp. 1454–1460, Nov. 1984.

[11] P. Espes, P. F. Combes, J Goutoule, and B. Theron, "Asymmetrical finline for space applications using millimeter waves," *IEEE Trans. Microwave Theory Tech.*, vol. 37, pp. 289–298, July 1989.

[12] T. Itoh, "Spectral domain immitance approach for dispersion characteristics of generalized printed transmission lines," *IEEE Trans. Microwave Theory Tech.*, vol. MTT-28, pp. 733–736, July 1980.

[13] L. P. Schmidt and T. Itoh, "Spectral domain analysis of dominant and higher order modes in fin-lines," *IEEE Trans. Microwave Theory Tech.*, vol. MTT-28, pp. 981–985, Sept. 1980.

[14] C. M. Bulter and R. Umashankar, "Electromagnetic penetration through an aperture in an infinite, planar screen separating two half spaces of different electromagnetic properties," *Radio Sci.*, vol. 11, no. 7, pp. 611–619, July 1976.

[15] T. Itoh and R. Mittra "A technique for computing dispersion characteristics of shielded microstrip lines," *IEEE Trans. Microwave Theory Tech.*, vol. MTT-22, pp. 896–898, Oct. 1974.

[16] E. G. Farr, C. H. Chan, and R. Mittra, "A frequency-dependent coupled-mode analysis of multiconductor microstrip lines with application to VLSI interconnection problems," *IEEE Trans. Microwave Theory Tech.*, vol. MTT-34, pp. 307–310, Feb. 1986.

[17] Y. Utsumi, "Variational analysis of ridged waveguide modes," *IEEE Trans. Microwave Theory Tech.*, vol. MTT-33, pp. 111–120, Feb. 1985.

[18] C. H. Chan, K. T. Ng, and A. B. Kouki, "Analysis of stripline and finline with finite metallization thickness and substrate holding grooves—A mixed spectral domain approach," to be submitted.

[19] R. Mittra and S. W. Lee, *Analytical Techniques in the Theory of Guided Waves*. New York: Macmillan, 1971, pp. 4–11.

**Chi Hou Chan** (S'86–M'86) attended Hong Kong Polytechnic and the City College of New York. He received the B.S. and M.S. degrees in electrical engineering from Ohio State University, Columbus, in 1981 and 1982, respectively, and the Ph.D. degree in electrical engineering from the University of Illinois, Urbana, in 1987.

From 1981 to 1982, he was a Graduate Research Associate at the ElectroScience Laboratory, Ohio State University. From 1987 to 1989, he was a Visiting Assistant Professor with the Electromagnetic Communication Laboratory in the Department of Electrical and Computer Engineering at the University of Illinois. In September 1989, he joined the University of Washington, Seattle, as an Assistant Professor. His research interests include numerical techniques in electromagnetics, frequency-selective surfaces, microwave integrated circuits, high-speed digital circuits, and wave propagation in anisotropic media for integrated optics applications.

Dr. Chan is an associate member of URSI Commission B.

**Kwong T. Ng** (S'78–M'79) received the B.Eng. (Hons.) degree from McGill University, Montreal, Que., Canada, in 1979, and the M.S. and Ph.D. degrees from Ohio State University, Columbus, in 1981 and 1985, respectively, all in electrical engineering.

From 1979 to 1984, he was with the ElectroScience Laboratory, Ohio State University, where he worked on numerical electromagnetics, phased arrays, frequency selective surfaces, and radomes. Since 1985, he has been with the University of Virginia, Charlottesville, where he is currently an Assistant Professor of Electrical Engineering. His current research interests include numerical electromagnetics, phased arrays, frequency selective surfaces, and millimeter-wave components.

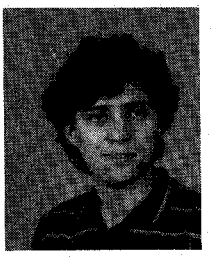

**Ammar B. Kouki** (S'88) was born in Téboursuk, Tunisia, on November 27, 1962. He received the B.S. and M.S. degrees in 1985 and 1987, respectively, from Pennsylvania State University, both in engineering science.

From September 1985 to May 1987, he was with the Research Center for the Engineering of Electronic and Acoustic Materials at Pennsylvania State University as a research assistant. Since August 1987, he has been with the Electromagnetic Communication Laboratory at the University of Illinois, where he is currently pursuing the Ph.D. degree. His current research interests include numerical electromagnetics, microstrip discontinuities, and radiation from printed-circuit boards.

Mr. Kouki has been a recipient of a national scholarship from the Tunisian government since 1981.